



Advanced Framework for Effective Denoising the Enhanced Thermal Breast Image

A. Arul Edwin Raj, M. Sundaram & T. Jaya

To cite this article: A. Arul Edwin Raj, M. Sundaram & T. Jaya (2021): Advanced Framework for Effective Denoising the Enhanced Thermal Breast Image, IETE Journal of Research, DOI: [10.1080/03772063.2021.1898481](https://doi.org/10.1080/03772063.2021.1898481)

To link to this article: <https://doi.org/10.1080/03772063.2021.1898481>



Published online: 14 Mar 2021.



Submit your article to this journal [↗](#)



Article views: 16



View related articles [↗](#)



View Crossmark data [↗](#)



Advanced Framework for Effective Denoising the Enhanced Thermal Breast Image

A. Arul Edwin Raj ¹, M. Sundaram² and T. Jaya ³

¹Electronics and Communication Engineering Department, Bethlahem Institute of Engineering, Karungal, India; ²Electronics and Communication Engineering Department, V.S.B. Engineering College, Karur, India; ³Electronics and Communication Engineering Department, C.S.I Institute of Technology, Thovalai, India

ABSTRACT

Nullifying the noise and redundancy in the breast thermogram is still a critical challenge. In this paper, a framework is designed for the purpose of classification of noisy RGB thermal breast images. The proposed framework includes enhancement in frequency domain, advanced mixed denoising and color correction for thermal images. The enhancement of thermogram uses curvelet transform that is applied to the V component of the HSV derived from RGB thermogram. Gain-controlled bi-histogram equalization operation is performed to the detailed component of V to enhance the image quality. The advanced mixed denoising algorithm is also presented using a combination of Gaussian and bilateral filter for denoising the enhanced thermogram. Spatially varying color correction (SVCC) technique is applied, which is based on an optimum linear color correction matrix that is calculated from the local blocks of enhanced image. The classification outcome of this proposed framework is more encouraging compared with the results of the existing methods for thermogram classification.

KEYWORDS

Breast thermogram; Curvelet transform; Color correction; Feature extraction; Image enhancement; Mixed denoising; SVM classifier

1. INTRODUCTION

Breast thermography, or breast thermal imaging, is a noninvasive and painless test. The physicians may refer the thermal breast images for early detection of malignancy. It works by identifying increases in temperature of the breast. Thermography does not involve any harmful radiation during image acquisition. Because of using a high-resolution thermal camera to map heat changes of the breast into images, the quality of thermogram is ensured more in the field of medical imaging. This thermal image has to be analyzed to identify breast abnormality by the temperature variation of the breast, it helps in early detection of breast cancer. When a tumor cell develops in an area, the human body will increase the blood flow of the area to rejuvenate the part which makes this area to become warmer. A tumor can be easily identified from the hot spot of the thermogram. The early detection of breast tumor increases the survival probability of the patient.

Thermogram has the limitation of low contrast, limited dynamic range, and poor visibility of the target from the background. Because of these types of limitations, it is difficult to retrieve the hidden information and edge identification of the dark region. Normally noises are robust and zero mean so that single operation such as image enhancement or color correction or

image denoising is not enough to improve the image fidelity. Hence it requires a platform to eradicate these limitations.

In the early literature, many algorithms have been proposed for color image enhancement and color correction, which include fuzzy nonlinear enhancement algorithm based on curvelet [1], nonlinear enhancement algorithm based on contourlet [2], fuzzy wavelet [3], ridgelet transform [4] and the neural network with a simple reflection model [5]. Even though these algorithms enhance the image quality, they also increase the noise. Hence the literature survey concentrated on denoising and image color correction algorithms. Color Correction is implemented by Root polynomial [6]. Rudin and Osher [7] examined a total variation minimization technique, but they have not considered the edges in their work. Similarly, Smith and Brady [8] described the smallest unvalued segment assimilating nucleus (SUSAN) filter for edge preservation, corner preservation and structure preservation with reduced noise. Lim and Silverstein [9] proposed spatially varying color correction (SVCC) that divided the image into 8 by 8 non-overlapping local blocks and calculated the correlation matrix for each channel and noise. The color correction matrix is computed directly from correlation matrix with the consideration of noise effect. While these algorithms control the

noise amplification, it could not remove the noise to the negligible amount. So, it needs a framework that is a combination of these processes such as denoising and color correction etc.

In this paper, an advanced framework for effective denoising of the enhanced thermal breast image is proposed. This work is an integration of three components. The first one is a color image enhancement approach where curvelet transform is applied to the V component of HSV raw image, which subdivides the image into base and detailed components. A bihistogram equalization approach is performed in detailed components to enhance the image quality and then the modified detailed components or coefficients are used to get an enhanced image after inverse curvelet transform. The second component of the framework is an advanced denoising technique for the enhanced thermal image where the combination of Gaussian and bilateral filters [10] is applied. The Gaussian filter extracts the reference image from the enhanced thermogram. Then the reference image and the enhanced images are given as the input of bilateral filter which gives an effective denoising in the resulted thermogram. The third one is image color correction which uses spatially varying color correction (SVCC) [9]. In the SVCC approach, the denoised image is decomposed into 8 by 8 local blocks to calculate the optimum linear color correction matrix. This color correction matrix is applied to the enhanced image for

color correction by applying optimum linear color correction matrix which was calculated from the local blocks of enhanced denoised thermogram.

The rest of this paper is composed as follows: Materials and method is described in section 2. Image enhancement using curvelet and gain-controlled bihistogram equalization method is explained in section 3. The advanced denoising algorithm is presented in section 4. Color correction with SVCC matrix is presented in section 5. The result and discussion of the proposed approach with the existing methods are presented in section 6. Finally, the conclusion is made for the proposed framework.

2. MATERIALS AND METHODS

Thermal images, collected from the Indira Gandhi Centre for Atomic Research (IGCAR) database, are subjected to undergo pre-processing in order to make the image more suitable for further image processing. In this work pre-processing is done to crop out the rest of the breast portion from the thermal image and also the images are resized into fixed size. Color image enhancement plays a vital role to get a reliable result at the final stage of this work.

The proposed approach, shown in Figure 1, initially converts the RGB thermal image into HSV image. HSV Color

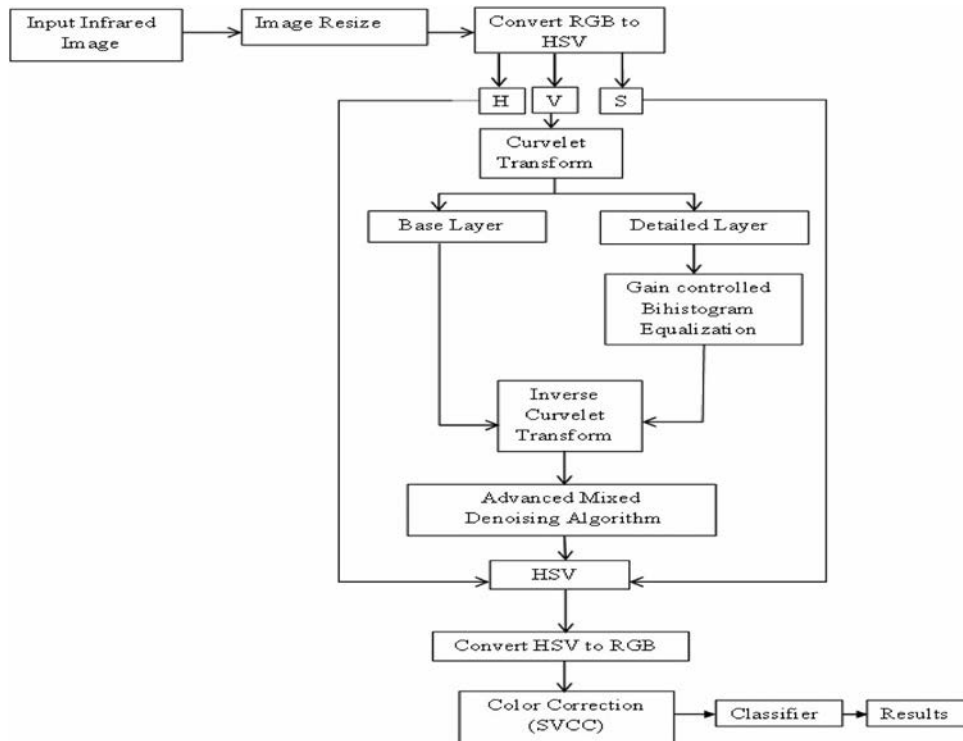


Figure 1: Block diagram of proposed workflow

Model has three components, which are Hue, Saturation and Value. Hue represents color of an object, it is also called tint.

Saturation indicates the purity of color, ranges from 0 to 100 percent. If the saturation is reduced toward zero, it increases gray level and pale the image quality. Value is also called as luminance: it defines the brightness or intensity of the each color, in the range of zero to 255. Zero stands for minimum brightness (black), while 255 is for the maximum brightness. Value is measured in candelas per square meter. In these three components, value component plays the vital role to maintain the image quality. Hence, in this approach the V components are only processed during the enhancement. Curvelet transform conserves edges and curves originalities much more efficiently than traditional Fourier and wavelet transforms. Applying curvelet transform, base and detailed layers are obtained from the given V component. The base layer has the low-frequency approximation components and the detailed layer has the high-frequency coefficients. Hence the proposed approach employed gain-controlled bihistogram equalization algorithm to modify the values of the coefficients in the detailed sub-bands. After this process the base and detailed layers are used for reconstruction using inverse curvelet transform to get enhanced image. Furthermore, this enhanced HSV image is denoised using an advanced mixed denoising algorithm. The advanced mixed denoising algorithm is the combination of Gaussian and bilateral filter operations. In the mixed denoising filter, the Gaussian filter smoothens all the regions in the image with the same probability and bilateral filter is used to preserve the edges.

Then this processed V component is combined with H and S components to get an enhanced HSV image which is converted back to RGB image. The final color correction process is an important color image processing operation that converts a camera-dependent RGB color model into a standard color model. The thermal image color correction is performed by multiplying processed RGB values of the denoised thermogram by a color correction matrix which is calculated from the image. It [11] is learned from the literature that even though the color correction method improves the color quality of the image, it also amplifies the image noise. In order to overcome this challenge, [9] SVCC approach has been used in this work for achieving better color correction.

Finally, the above processed thermograms are classified into normal and abnormal images by extracting seven

statistical parameters, namely; Entropy, PSNR, Mean, Variance, Standard deviation, Energy and Correlation.

3. IMAGE ENHANCEMENT

Image enhancement stage tries to improve the visible appearance of a thermal image or to convert the thermogram to a form which would be more appropriate for analysis by a machine or human [12]. In the proposed approach the RGB thermal image in the database is converted into the HSV image. In the HSV color image enhancement, Hue (H) and Saturation (S) components should not be altered because H and S components are responsible for color maintenance [13,14]. If H and S of the images are changed, they affect the original color of the image and lead to false diagnosis in the later stage. Therefore, this proposed method concentrates on the manipulation of Value (V) component. The V component of the thermogram is undergone curvelet transform and gain-controlled bihistogram equalization approach for the manipulation of coefficients.

3.1 Curvelet Transform

Curvelet transform is the better option to overcome the poor directivity of traditional wavelet and Fourier transforms. Its multi-scale geometry property preserves the edges and curves singularities much more efficiently than the latter ones.

General form of discrete curvelet transform is represented as

$$C(k, \theta, k_1, k_2) = \sum_{\substack{0 \leq i \leq M \\ 0 \leq j \leq N}} I(i, j) \Phi_{j, \theta, k_1, k_2}[i, j] \quad (1)$$

where k is the scale which indicates the number of levels, θ is the Orientation, k_1, k_2 are the Spatial locations of curvelet function, $\Phi [i, j]$ is the curvelet function, $I (x, y)$ is the input image having dimension M, N and $\Phi_{k, \theta, k_1, k_2}[i, j]$ is the curvelet function, it is the extension of the ridgelet transform to multiple scale analysis [15].

Curvelet Transform uses orientation scales to separate high-frequency domain sub-bands. In scale 2 it separates 16 orientations detailed sub-bands, in scale 3 it is divided into 32 sub-bands and these sub-band divisions continues like this. This sub-band coefficient preserves edges within an image more effectively. Equation (1) represents curvelet transform and it

can also be implemented in an alternative approach as follows.

Curvelet transform

$$= I_{nn} \text{FFT}\{\text{FFT}([\emptyset[i, j]]) \times \text{FFT}(I(i, j))\} \quad (2)$$

Trapezoidal shape wedge frequency response of Curvelet transform cannot applied in the frequency spectrum directly to obtain inverse FFT. So this wedge needs to be wrapped into a rectangular response periodically. Then these rectangular responses are applied into the thermogram frequency spectrum directly and the rectangular coefficient areas under this origin are collected. Because of this wedge wrapping process, curvelet transform is also known as the wrapping-based curvelet transform.

3.2 Gain-Controlled Bihistogram Equalization

A detailed layer is enhanced using adaptive gain control weighting function $W(i, j)$

$$W(i, j) = \frac{1}{|w|} \sum_{(m,n) \in W_{i,j}} \left(\frac{(I(i, j) - \mu_{m,n})^2}{\sigma_{m,n}^2 + \epsilon^l} \right) \quad (3)$$

where $W(i, j)$ – kernel function of adaptive gain control, w – number of pixel in the kernel window $W(i, j)$, $I(i, j)$ – Sub-band image, $\mu_{m,n}$ – Mean of sub-band Image $I(i, j)$, $\sigma_{m,n}^2$ – Variance of sub-band image $I(i, j)$, ϵ^l – parameter need to be modified for enhancement, $I_{G(i,j)}$ – Gain-controlled sub-band image

For a completely low-frequency region, the value of $W(i, j)$ is near 0. It increases with the frequent changes of the pixel. From the available research literature, it is learned that most of the values in $W(i, j)$ should be equal to 1 and maximum value of $W(i, j)$ is assigned to 1.2 in such a way the value of ϵ^l is selected.

$$I_{G(i,j)} = I(i,j) * w(i, j) \quad (4)$$

Then the gain-controlled image $I_{G(i,j)}$ is undergone bihistogram equalization process, it divides the image $I_{G(i,j)}$ into two sub-images based on the mean of the image. These subdivided images are histogram equalized separately and joined together to improve the thermal image visibility which leads better results for further process.

$I_{GL(i,j)}$ and $I_{GU(i,j)}$ are subdivided images. $I_{GM(i,j)}$ is the rounded mean intensity of the image. $I_{GL(i,j)}$ $I_{GU(i,j)}$ are sub-images whose intensity is less than and greater than

the mean intensity $I_{GM(i,j)}$, respectively

$$I_{G(i,j)} = I_{GL(i,j)} \cup I_{GU(i,j)} \quad (5)$$

The probability density function of sub-images is

$$P(I_{GL(i,j)}) = n^k / n_L \quad (6)$$

where $k = 0, 1, 2, \dots, I_{GM(i,j)}$

$$P(I_{GU(i,j)}) = n^k / n_u \quad (7)$$

where $k = I_{GM(i,j)} + 1, I_{GM(i,j)} + 2, \dots, L - 1$

The cumulative density function of sub-images is

$$C(I_{GL(i,j)}) = \sum_{J=0}^{I_{GM(i,j)}} P_J(I_{GL(i,j)}) \quad (8)$$

and

$$C(I_{GU(i,j)}) = \sum_{J=I_{GM(i,j)}+1}^{L-1} P_J(I_{GU(i,j)}) \quad (9)$$

$F(I_{G(i,j)})$ is the transform function of gain-controlled enhanced bihistogram thermal image. It rebuilds the enhanced thermogram based on cumulative distribution functions and output thermogram of the histogram equalization.

3.3 Gain-Controlled Bihistogram Equalization Algorithm

Step 1: Base and detailed layers of thermal images are separated using curvelet transform.

Step 2: Adaptive gain control weight function $W(i, j)$ is calculated.

Step 3: $W(i, j)$ is applied on the detailed layer to obtain I_G .

Step 4: Threshold (I_{GM}) is identified from the histogram of I_G .

Step 5: I_G grouped into two as follows:

$$I_{GU}: \text{pixel intensity} > I_{GM}.$$

$$I_{GL}: \text{pixel intensity} \leq I_{GM}.$$

Step 6: Probability Density Function (PDF) is calculated separately for I_{GU} and I_{GL} .

Step 7: Cumulative Density Function (CDF) is calculated separately for I_{GU} and I_{GL} .

Step 8: Transform function $F(I_G)$ is calculated from CDF and histogram thermal image.

Step 9: Enhanced detailed layer of thermogram is rebuilt using transfer function $F(I_G)$.

Step 10: Base layer and detailed layers are recombined using inverse curvelet transform.

4. ADVANCED MIXED DENOISING ALGORITHM

The Gaussian filter can't preserve the edges because of its linear operation; and also its standard deviation manages the degree of smoothening. During the smoothening operation, it handles the entire image region with equal priority, including edges or details and also it blurs the image [16]. The bilateral filter is just opposite of this; it's a non-linear filter [10]. It avoids averaging across image edges while averaging within smooth regions of the image; thus, it preserves edges. But the bilateral filters have the drawbacks of non-iterative and staircase effect creation. To overcome the above issues, an advanced mixed image de-noising algorithm is used based on Gaussian filter and bilateral filtering. It removes the noise while retaining the important image features like edges, details as much as possible. It behaves linearly in the smooth region of the image and nonlinearly in the edges.

In the Gaussian filter, the kernel has a strong central pixel weight and gradually decreases toward the edge. Its function is defined as in equation (10)

$$G_\sigma(x, y) = \frac{1}{2\pi\sigma^2} e^{-\frac{(x^2+y^2)}{2\sigma^2}} \quad (10)$$

The Gaussian filters smoothen the image spatial variations, control the noise and preserves image features by the mean value of local neighborhood pixels. This operation is working well in the low frequencies, but it misses the high-frequency edges.

Bilateral filter overcomes Gaussian drawbacks by smoothening the images while preserving edges. Bilateral filter function at a pixel location l is defined as in the following equation.

$$I_B(l) = \frac{1}{W} \sum_{m \in S} G_{\sigma_s}(\|l - m\|) G_{\sigma_r}(|X(l) - I(m)|) I(m) \quad (11)$$

where $G_{\sigma_s}(\|l - m\|) = e^{-\frac{\|l - m\|^2}{2\sigma_s^2}}$ is the geometric closeness function, $G_{\sigma_r}(|X(l) - I(m)|) = e^{-\frac{|X(l) - I(m)|^2}{2\sigma_r^2}}$ is the

gray level similarity function, $W = \sum_{m \in S} G_{\sigma_s}(\|l - m\|) G_{\sigma_r}(|X(l) - I(m)|)$ is the normalized constant, $\|l - m\|$ is the Euclidean distance between l and m and S is the spatial neighborhood of m .

The two parameters σ_s and σ_r define the function of the bilateral filter.

The advanced mixed image de-noising algorithm is the combination of Gaussian and bilateral filters. First, the Gaussian filter is applied to the enhanced V component of the HSV image which is treated as a reference image for the bilateral filter. Next, the kernel function is taken from the reference image, the kernel function and image to be enhanced is given as the input of the bilateral filter. The low-frequency and high-frequency components can be provided by reference and image to be denoised, respectively.

$$X^{(t+1)}(l) = \frac{1}{W} \sum_{m \in S} G_{\sigma_s}(\|l - m\|) G_{\sigma_r}(|X^t(l) - I(m)|) I(m) \quad (12)$$

$$IIF(l) = \sum_{m \in S} G_{\sigma_s}(\|l - m\|) G_{\sigma_r}(|X^t(l) - I(m)|) \quad (13)$$

In Equations (12) and (13) $G_{\sigma_s}(\cdot)$ represents a spatial kernel function, $G_{\sigma_r}(\cdot)$ represents a range kernel function, and σ_s and σ_r determine the expansion degree of spatial kernel function and range kernel function, respectively.

The bilateral filter function is represented in Equation (11) and used to solve the non-iterative and staircase effect problem, it can be converted into a mixed denoise equation, represented by the Equations (12) and (13). Here it takes the values of $t=0-255$. In order to implement Equation (13) the initial value of $X_p(1)$ is considered as $X_p(1) = I_p$, then the iterative computation is performed only once.

5. COLOR CORRECTION

In this paper, Color correction matrix is used to reproduce the optimum image from the high dynamic range camera (processed) image. The dynamic range of thermal images received from the camera differs from the dynamic range of the human visual system. This process maintains the color fidelity and makes the image more suitable than the results without color correction. In this work, a Spatially Varying Color Correction (SVCC) with linear 3×3 color correction matrix [9] is presented.

Generally, the color images are represented as $R \times C \times 3$ (R rows, C columns, and 3 color components). For simplicity during mathematical representation, the color image is considered as $K \times 3$ arrays, where $K = R \times C$. The image before color correction (UI) can be represented as

$$UI = \begin{bmatrix} UI_{R1} & UI_{G1} & UI_{B1} \\ UI_{R2} & UI_{G2} & UI_{B2} \\ \vdots & \vdots & \vdots \\ UI_{RK} & UI_{GK} & UI_{BK} \end{bmatrix} \quad (14)$$

where

$[UI_{Ri}, UI_{Gi}, UI_{Bi}]$ is the normalized R, G, and B values of i th row, respectively. The transformed (color corrected) array is called CI, which is achieved by matrix multiplication with C and M (3×3), the color-corrected image is represented as

$$CI = UI * CM \quad (15)$$

where UI: uncorrected image; CI: color corrected image; CM: color correction matrix.

Color correction matrix CM is obtained by solving the sum-of-square difference between ideal and color corrected spectral sensitivity function [17]. In a practical situation, the uncorrected image may contain noise, so the CM mapping often amplifies [18] the noise also. This noise can be eliminated by an optimal linear mapping [11,19] by focusing the color corrected image, color accuracy, and the noise.

The optimal linear mapping matrix is estimated as

$$OLM = \arg \min_{CM_n} E[\| CMUI - CM_n UI_n \|] \quad (16)$$

where OLM is the optimum Linear Matrix, $UI_n = [r_n, g_n, b_n]^T$ is the noisy RGB vector, $E[\cdot]$ is the expectation operation.

In some cases the noises are non-zero Gaussian noise. This is independent of RGB signals and independent of each other, so the optimal linear matrix is modified as follows

$$OLM = CM(C - C^n)^T (C^{-1})^T \quad (17)$$

where C and C^n are the correlation matrix of the noisy RGB vector and correction matrix of noise, respectively.

$$C = \begin{bmatrix} E[r_n^2] & E[r_n g_n] & E[r_n b_n] \\ E[r_n g_n] & E[g_n^2] & E[g_n b_n] \\ E[r_n b_n] & E[g_n b_n] & E[b_n^2] \end{bmatrix} \quad (18)$$

$$C^n = \text{diag}([\sigma_r^2, \sigma_g^2, \sigma_b^2]) \quad (19)$$

where $[\sigma_r^2, \sigma_g^2, \sigma_b^2]$ are the noise variances of the RGB channel.

In SVCC the noise image is divided into 8×8 blocks. Then the correlation matrix is computed for each block separately, next color correction matrix is calculated from the correlation matrix. This color correction matrix is applied to all pixels of the noisy image. From the experimental analysis, it is understood that the SVCC can control the noise amplification with excellent image quality.

6. RESULT AND DISCUSSION

The V component of raw HSV thermal breast image is given as the input of curvelet transform with scale 3. In scale 2 it divides the image into one approximation component and 16 detailed components in 16 different orientations. In scale 3 it divides into 32 detailed components. The following is one of the examples of approximation and detailed components for scale 3.

Figure 2(a) shows left breast thermogram of abnormal case name Alamelu. In this proposed work Curvelet transform is applied in the V component of this thermogram in scale 3. It separates the V component into one approximation coefficient and 32 detailed coefficients which are shown in Figure 2(b) and Figure 3, respectively.

Figure 4 shows the stage by stage result of the proposed framework for three abnormal cases named Alamelu, Andal and Dhanalakshmi. Figure 5 shows staged by stage result of the proposed framework for four normal cases named Amutha, Banu, Banumathi and Candra.

6.1 Quantative Analysis

Quantitative analysis is carried out for comparison of different stages of the proposed work. For this analysis

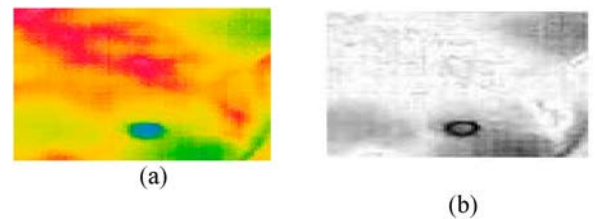


Figure 2: Thermogram of left breast and corresponding V component approximation curvelet coefficient in scale 3 of abnormal case name Alamelu. (a) Thermogram (b) Approximation coefficient

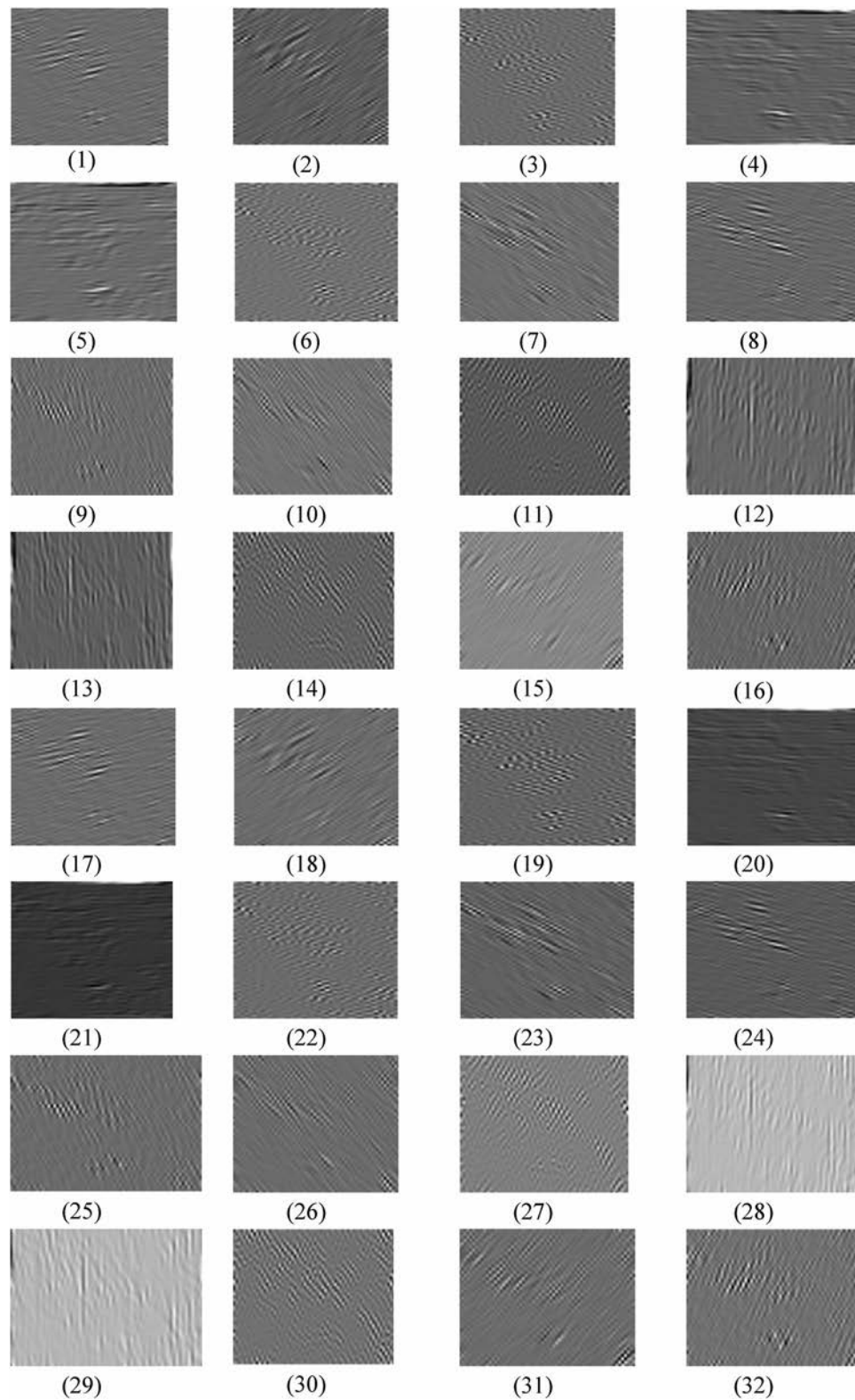


Figure 3: 32 different detailed subband curvelet coefficient for scale

following seven [20] statistical features are extracted based on GLCM, PCA. The statistical features are entropy, PSNR, mean variance, standard deviation, correlation and energy.

6.2 Experimental Analysis

In Figure 6(a-d) the energy and correlation features of normal and abnormal cases are compared and it is understood that the proposed work output of the

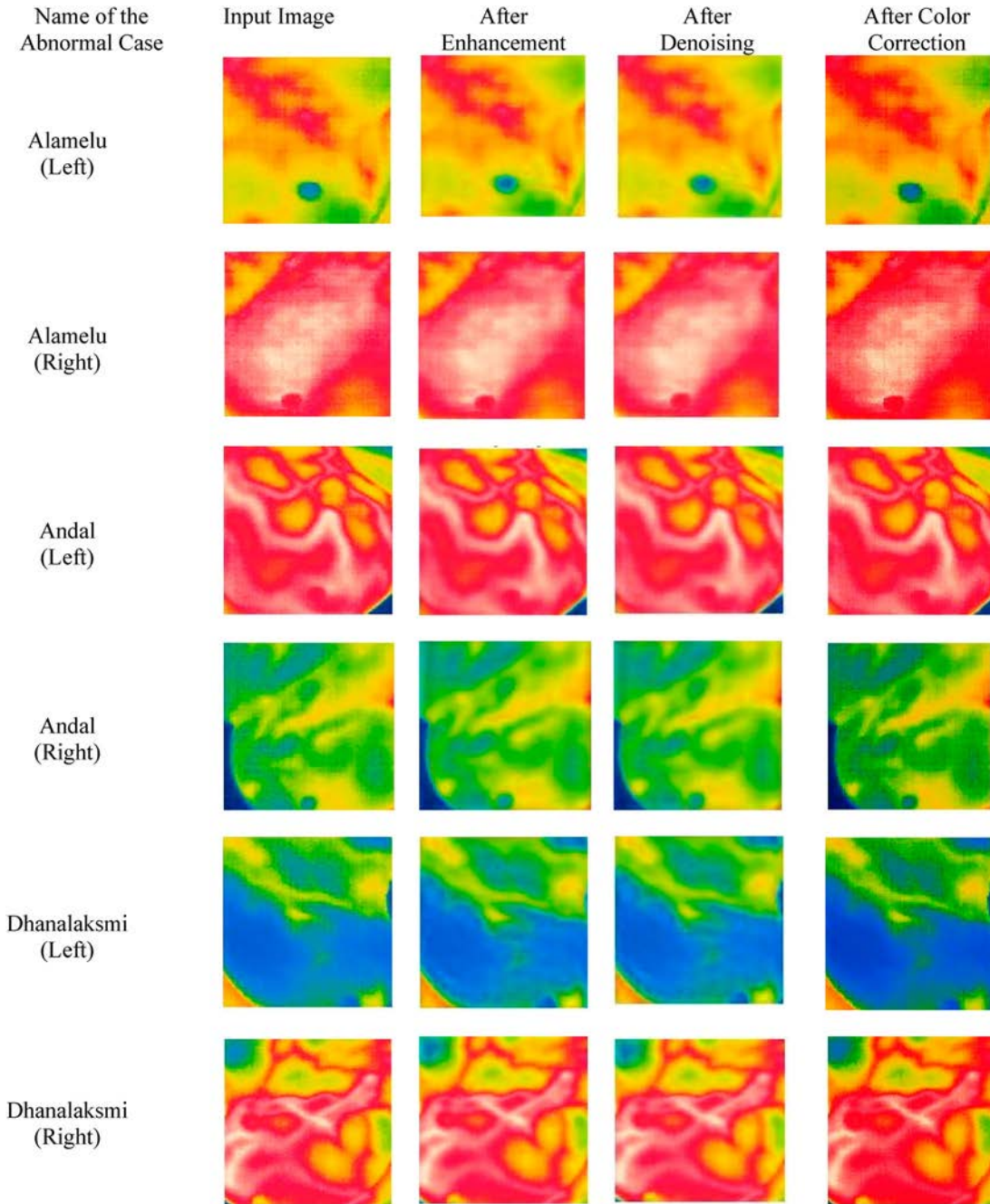


Figure 4: Stage by stage result of the proposed framework for three abnormal cases

normal case is more consistent than the abnormal. Figure 7(a,b) give a comparison of the standard deviation feature for abnormal and normal case, respectively, were also the normal case feature is consistent for various persons. From Figure 7(c,d) it is observed that the variance feature for the abnormal case is more consistent than the normal case. From Figure 8(a–d), Figure 9(a,b) shows the Entropy, PSNR and Mean comparison here both the normal and abnormal case are consistent but in two different levels (Tables 1 and 2).

From the above discussion, it is witnessed that the above said 7 consistent features can be used as the training features for SVM classifies; it will help the classifier to fix the hyperplane exactly. The considerable gap between the consistent and inconsistent features guides the classifier to fix the exact location of the hyperplane.

6.3 Evaluation Metrics

For classification performance evaluation, the available thermograms of IGCAR dataset have been used. A total

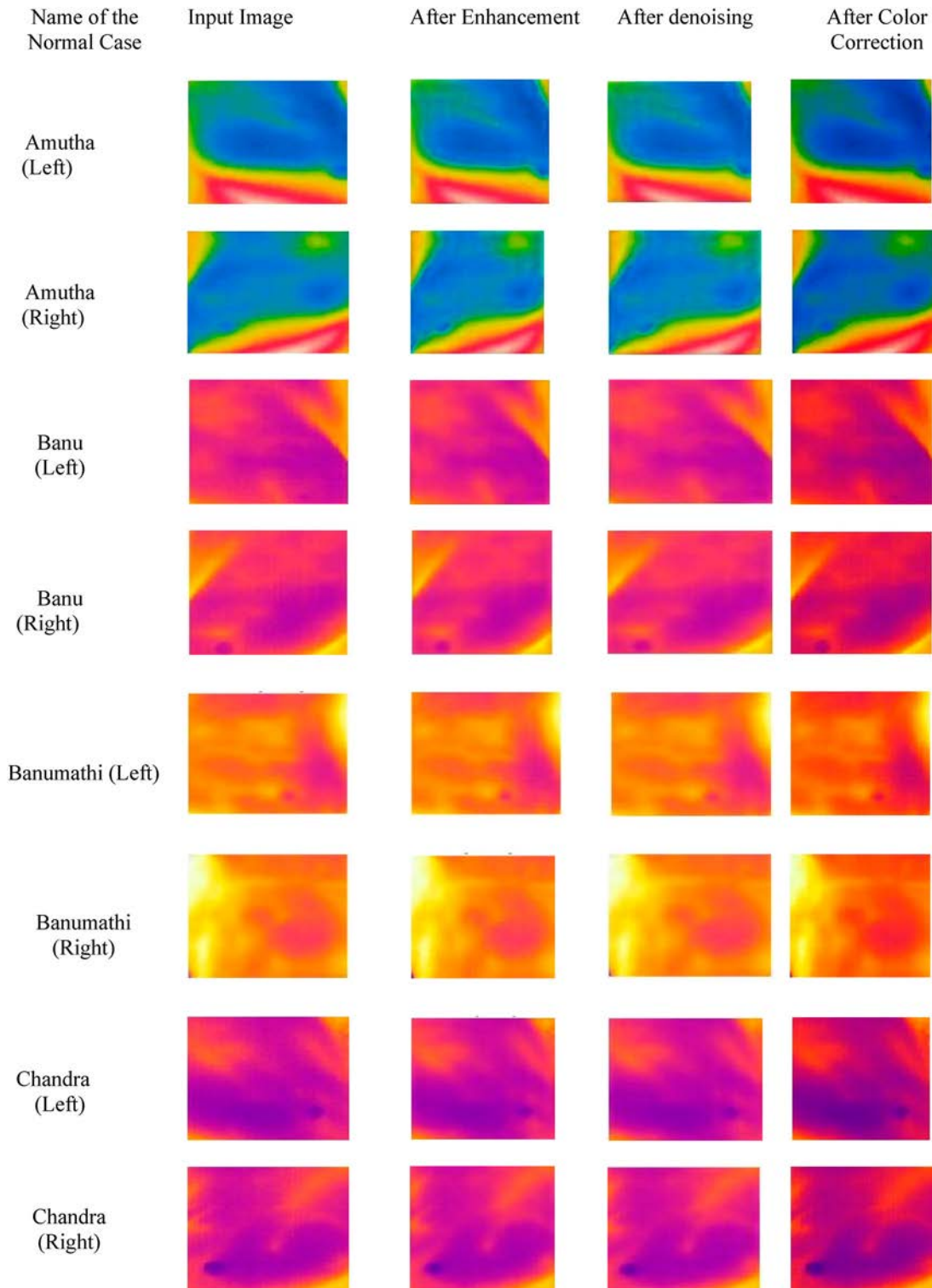


Figure 5: Stage by stage result of the proposed framework for four normal cases

of 80 thermography images of the breast including 48 normal and 32 malignant are analyzed. The ten statistical features are extracted based on GLCM, PCA and seven features are found to be statistically significant for fixing the hyperplane by SVM classifier. Every

statistical feature value is calculated as the average of values obtained from the four GLCM matrices with one distance $d = 1$ pixel. The classifiers employed in this research are support Vector Machine which is trained by a feature vector and tested from the IGCAR

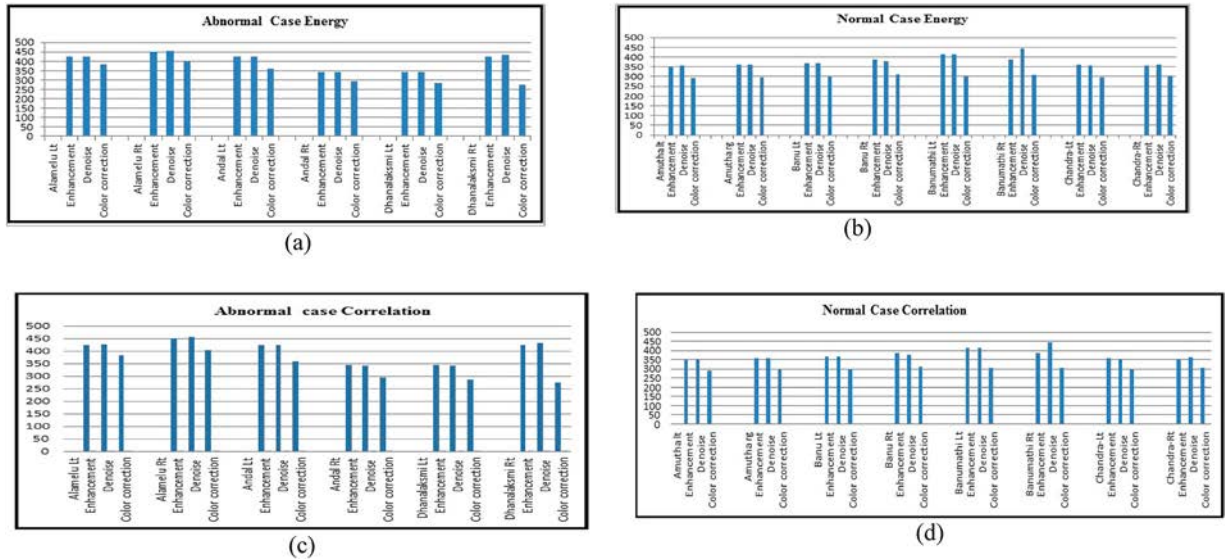


Figure 6: Stage by stage energy and correlation features comparison chart for both normal and abnormal cases. (a) Abnormal case energy (b) Normal case energy (c) Abnormal case correlation (d) Normal case correlation

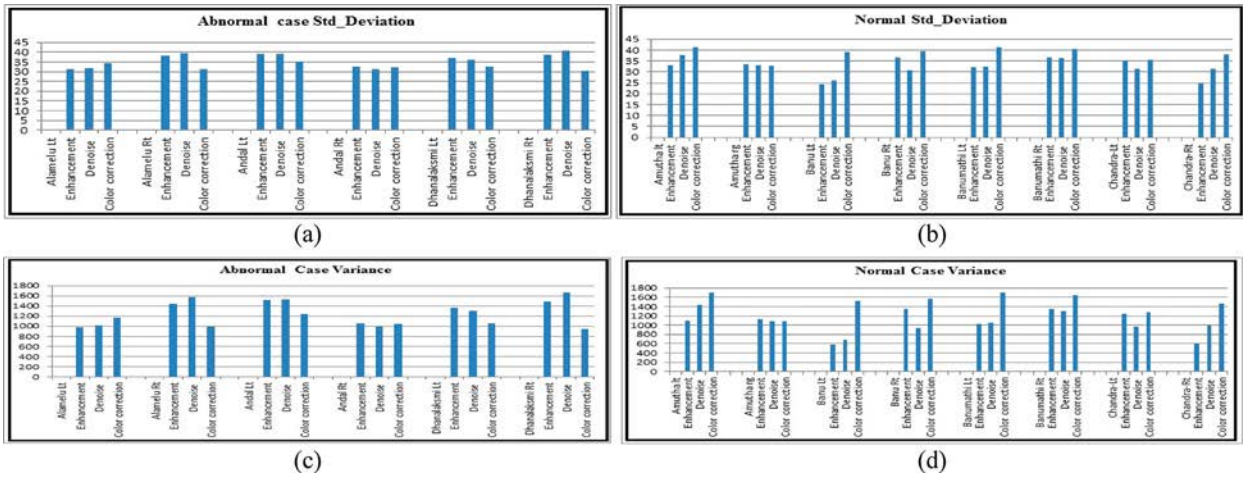


Figure 7: Stage by stage standard deviation and Variance features comparison chart for both normal and abnormal cases. (a) Abnormal case standard deviation (b) Normal case standard deviation (c) Abnormal case variance (d) Normal case variance

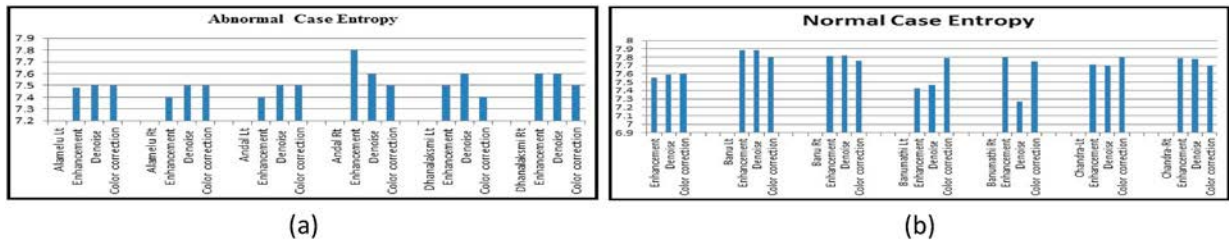


Figure 8: Stage by stage entropy and PSNR features comparison chart for both normal and abnormal cases. (a) Abnormal case entropy (b) Normal case entropy (c) Abnormal case PSNR (d) Normal case PSNR

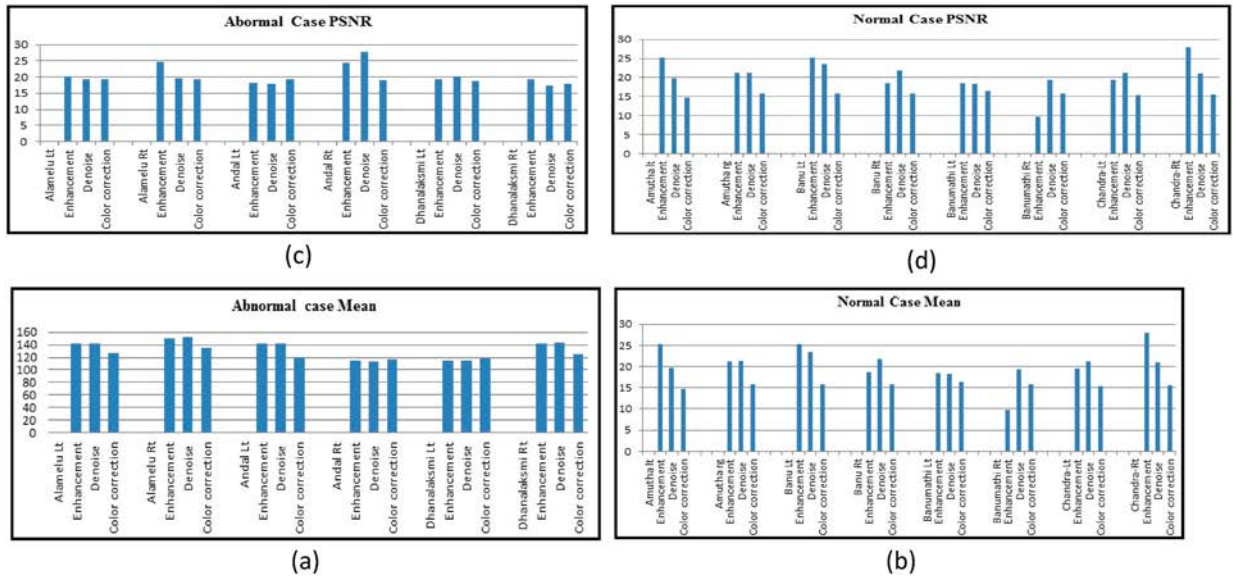


Figure 9: Stage by stage Mean features comparison chart for both normal and abnormal cases. (a) Abnormal case Mean (b) Normal case Mean

Table 1: Statistical features extracted from three Stages of proposed work for abnormal cases

Name	Abnormal Case						
	Entropy	PSNR	MEAN	VARIANCE	STD. DIVIATION	ENERGY	CORRELATION
Alamelu Lt							
Enhancement	7.48	20.15	141.17	978.4384	31.28	423.52	0.87
Denoise	7.5	19.3	142	1011.24	31.8	426	0.8
Color correction	7.5	19.2	127.6	1162.81	34.1	382.7	0.9
Alamelu Rt							
Enhancement	7.4	24.8	150.3	1444	38	450.8	1
Denoise	7.5	19.5	152.1	1576.09	39.7	456.2	0.8
Color correction	7.5	19.3	134.4	992.25	31.5	403.2	0.9
Andal Lt							
Enhancement	7.4	18.1	141.4	1521	39	424.3	0.7
Denoise	7.5	17.9	141.5	1528.81	39.1	424.5	0.7
Color correction	7.5	19.3	120	1239.04	35.2	359.9	0.9
Andal Rt							
Enhancement	7.8	24.3	115.5	1049.76	32.4	343.5	0.9
Denoise	7.6	27.84	114.19	989.1025	31.45	342.5	0.9
Color correction	7.5	19.1	116.3	1043.29	32.3	294.8	0.7
Dhanalaksmi Lt							
Enhancement	7.5	19.4	114.6	1361.61	36.9	343.7	0.8
Denoise	7.6	20.2	114.4	1303.21	36.1	343.1	0.8
Color correction	7.4	18.9	118.9	1049.76	32.4	284.8	0.8
Dhanalaksmi Rt							
Enhancement	7.6	19.38	141.65	1492.277	38.63	424.96	0.8
Denoise	7.6	17.3	144.1	1664.64	40.8	432.4	0.8
Color correction	7.5	17.9	124.5	936.36	30.6	273.6	0.9

data base. Using this technique, 30 images are used for training and remaining for testing [21,22]. This is then repeated for different enhancement stages in this work.

The classification performance is assessed by the metrics such as Sensitivity, Accuracy, Specificity, FPR (False Positive Rate) and TPR (True Positive Rate) and it is defined as in equation (20–24).

6.3.1 Sensitivity

Measures the proportion of positive cases which are correctly identified as positive

$$\text{Sensitivity} = \frac{TP}{TP + FN} \quad (20)$$

6.3.2 Accuracy

Percentage of correct classification

$$\text{Accuracy} = \frac{TP + TN}{TP + TN + FP + FN} \quad (21)$$

Table 2: Statistical features extracted from three Stages of proposed work for abnormal cases

Name	Normal Case						
	Entropy	PSNR	MEAN	VARIANCE	STD. DIVIATION	ENERGY	CORRELATION
Amutha Lt							
Enhancement	7.63	25.29	115.8705	1090.796	33.0272	347.6115	0.94
Denoise	7.68	19.68	118.71	1431.866	37.84	356.14	0.79
Color correction	7.6	14.8	98	1705.69	41.3	294	0.8
Amutha Rt							
Enhancement	7.5532	21.1732	120.1084	1121.232	33.4848	360.3251	0.8228
Denoise	7.5904	21.2596	119.9218	1087.535	32.9778	359.7654	0.8224
Color correction	7.6	15.8	100	1755.61	41.9	295	0.8
Banu Lt							
Enhancement	7.8837	25.26	122.63	586.1241	24.21	367.9054	0.87
Denoise	7.8834	23.463	123.3053	684.9265	26.1711	369.9158	0.8391
Color correction	7.8	15.7	105.9	1521	39	298.9	0.8
Banu Rt							
Enhancement	7.8122	18.5848	134.7	1347.727	36.7114	386.9298	0.7122
Denoise	7.8224	21.7952	126.2041	937.8416	30.6242	378.6124	0.8095
Color correction	7.7606	15.8429	104.2021	1563.372	39.5395	312.6064	0.81
Banumathi Lt							
Enhancement	7.4288	18.5378	137.7322	1027.645	32.0569	413.1967	0.7499
Denoise	7.4679	18.3101	138.2311	1054.074	32.4665	414.6934	0.7751
Color correction	7.7921	16.4271	105.1889	1700.012	41.2312	304.55	0.82
Banumathi Rt							
Enhancement	7.8	9.7	129	1346.89	36.7	386.9	0.4
Denoise	7.2701	19.2967	148.4685	1306.222	36.1417	445.4054	0.8748
Color correction	7.7518	15.786	102.5292	1644.521	40.5527	307.5875	0.8211
Chandra Lt							
Enhancement	7.7059	19.4605	119.9943	1243.098	35.2576	359.9828	0.6626
Denoise	7.7009	21.1743	118.4262	972.3545	31.1826	355.2787	0.7128
Color correction	7.8	15.3	100	1274.49	35.7	296.69	0.8
Chandra Rt							
Enhancement	7.7875	27.9308	118.5037	601.1421	24.5182	355.511	0.9264
Denoise	7.7808	21.002	120.7093	989.6687	31.459	362.1279	0.7253
Color correction	7.7	15.6	101.7	1459.24	38.2	305	0.8

Table 3: Performance comparison of breast cancer detection approaches employing thermograms

Authors (Year)	Database	Features	Classifier	Accu (%)	Sens (%)	Spec (%)
Madhavi and Thomas [23]	DMR database (32-normal and 31-abnormal)	GLCM, GLRLM, GLSZM and NGTDM texture features	LSSVM	96	100	92
Abdel-Nassera, et al. [24]	DMR- IR database (37 - normal and 19-abnormal)	GLCM texture features	MLP	95.8	97.1	94.6
Ramya Devi and Anandhamala [25]	DMR database (35-normal and 25-abnormal)	GLCM texture features	SVM-RBF	95	97.05	92.3
Josephine Jeyanathan et al. [26]	DMR database (40sincluding normal and abnormal)	GLCM, WTB,2D-DDTWT, GWT, CT based texture features	GDA, KNN, NB, LR	91	87	90
Proposed method (Without Color Correction)	IGCAR (48-normal and 32-abnormal)	GLCM	SVM	91.6	90	87
Proposed method (With Color Correction)	IGCAR (48-normal and 32-abnormal)	GLCM	SVM	95.3	96.2	94.7

6.3.3 Specificity

Specificity is the estimation of negative cases which are properly recognized as negative

$$\text{Specificity} = \frac{TN}{TN + FP} \quad (22)$$

6.3.4 False-Positive Rate (FPR)

The false-positive rate is also called miss rate, which can be calculated by

$$\text{FPR} = \frac{FP}{FP + TN} \quad (23)$$

6.3.5 True-Positive Rate (TPR)

The true-positive rate is also called sensitivity, which is calculated as

$$\text{TPR} = \frac{TP}{TP + FN} \quad (24)$$

where TP is True Positive, TN is True Negative, FP is False Positive and FN is False Negative (Table 3).

7. CONCLUSION

In this work, in order to improve the classification accuracy of the thermograms, a new framework is

presented. Two approaches are introduced in this work; at first gain-controlled bihistogram threshold operator-based curvelet transform enhancement is implemented. The threshold on curvelet transform detailed sub-band coefficients has improved significant enhancement on thermograms which made more discriminable feature extraction suitable for classification. Second one is the advance mixed denoising approach to remove the noise in the enhanced thermogram. The novelty of this noise removal process is to preserve both low-frequency and high-frequency components during denoising. Finally, the demonised image is applied to the spatially varying color correction matrix to enrich the color of the image. Based on the performance analysis of the processed image about seven features are considered to be suitable for expected response from the classifier. So these seven features are considered as the training parameters for the classifier that support for the early detection of breast cancer. Experimental results of the proposed framework achieve encouraging improvements in accuracy about 95.3% compared to the existing classification methods.

ACKNOWLEDGEMENTS

We thank Indra Gandhi Centre for Atomic Research (IGCAR) for their assistance in data acquisition. We also thank the anonymous referees for their useful suggestions and support. We would like to thank our family, colleague and friends for their constant source of inspiration.

ORCID

A. Arul Edwin Raj  <http://orcid.org/0000-0002-7563-1144>

T. Jaya  <http://orcid.org/0000-0002-5920-9007>

REFERENCES

1. J. Zhao, and S. QU, "The Fuzzy nonlinear Enhancement algorithm of infrared image based on curvelet transform," *ELSEVIER Adv. Control Eng. Inf. Sci., Procedia Eng.*, Vol. 15, pp. 3754–8, 2011.
2. D. Shi, L. Qingwu, N. Xue, and H. Guanying, "Infrared Image nonlinear enhancement algorithm based on contourlet transfor," *Acta Optical Sinica*, Vol. 29, no. 2, pp. 342–6, Feb. 2009.
3. L. Guojun, T. Xianglong, and H. Jianhua, "An image contrast enhancement approach based on Fuzzy wavelet," *Acta Electron. Sin.*, Vol. 33, no. 4, pp. 643–6, Dec. 2005.
4. W. Gang, X. Liang, and H. Anzhi, "Algorithm research of adaptive Fuzzy image enhancement in Ridgelet Transform domain," *Acta Optical Sinica*, Vol. 27, no. 7, pp. 1183–90, Jul. 2007.
5. Y. S. Moon, B. G. Han, and H. S. Yang, "Low contrast image enhancement using convolutional neural network with simple reflection model," *Adv. Sci., Technol. Eng. Syst. J.*, Vol. 4, no. 1, pp. 159–64, Feb. 2019.
6. G. D. Finlayson, M. Mackiewicz, and A. Hurlbert, "Colour correction using root-polynomial regression," *IEEE Trans. Image Process.*, Vol. 24, no. 5, pp. 1460–70, May 2015.
7. L. Rudin, and S. Osher, "Total variation based image restoration with free local constraints," *Proc. IEEE Int. Conf. Image Process.*, Vol. 1, pp. 31–5, 1994.
8. S. M. Smith, and J. M. Brady, "Susan: a new approach to low level image processing," *Int. J. Comput. Vision*, Vol. 23, no. 1, pp. 45–78, May 1997.
9. S. Lim, and A. Silverstein. "Spatially varying color correction (SVCC) matrices for reduced noise," *Proc. of Color and Imaging Conference (CIC)*, pp. 76–81, Jan. 2004.
10. B. K. Shreyamsha Kumar, "Image denoising based on Gaussian/bilateral filter and its method noise thresholding," *Signal. Image. Video. Process.*, Vol. 7, pp. 1159–72, May 2013.
11. Y. P. Tan, and T. Acharya, "A method for color correction with noise consideration," *Proc. of SPIE*, Vol. 3963, pp. 329–37, Dec. 1999.
12. F. Lai, J. Kandukuri, B. Yuan, Z. Zhang, and M. Jin "Thermal image enhancement through the deconvolution methods for low-cost infrared cameras," *Quant. Infr. Therm J.*, Vol. 15, no. 2, pp. 1–17, May 2018.
13. R. Gonzalez, and R. Woods. *Digital image processing*. 3rd ed. Upper Saddle River, NJ: Prentice-Hall, 2007.
14. Q. Song, Y. Wang, and K. Bai, "High dynamic range infrared images detailed enhancement based on local edge preserving filter," *Infrared Phys. Technol.*, Vol. 17, pp. 464–73, Jul. 2016.
15. J. L. Starck, E. J. Candès, and D. L. Donoho, "The curvelet transform for image denoising," *IEEE Trans. Image Process.*, Vol. 11, no. 6, pp. 670–84, 2002.
16. K. Takahashi, Y. Monno, M. Tanaka, and M. Okutomi. "Effective color correction pipeline for a noisy image," *IEEE International Conference on Image Processing (ICIP)*, pp. 4002–6, Aug 2016.
17. U. Barnhofer, J. DiCarlo, B. Olding, and B. A. Wandell. "Color estimation error trade-offs," *Proc. SPIE Electron. Imaging Conf.*, Vol. 5017, pp. 263–73, May 2003.
18. P. Vora, and C. Herley. "Trade-offs between color saturation and noise sensitivity in image sensors," *Proc. IEEE Int. Conf. Image Process.*, Vol. 1, pp. 196–200, Nov. 1998.
19. S. Quan, "Analytical approach to the optimal linear matrix with comprehensive error metric," *Proc. of SPIE*, Vol. 5292, pp. 243–53, Jun. 2004.

20. X. Chen, Q. Zhang, and M. Lin, "No-reference color image quality assessment: from entropy to perceptual quality," *EURASIP J. Image Video Proc.*, Vol. 77, pp. 1–14, Sep. 2019.
21. J. Chakraborty, et al., "Computer-aided detection of mammographic masses using hybrid region growing controlled by multilevel thresholding," *J. Med. Biol. Eng.*, Vol. 39, pp. 352–66, May 2019.
22. V. Rajinikanth Suresh, S. Chandra Satapathy, and R. Nilanjan Dey. "DWT-PCA image fusion technique to improve segmentation accuracy in brain tumor analysis", *Microelectronics, Electromagnetics and Telecommunications*. Springer, Singapore, pp. 453–46, Jan. 2018.
23. V. Madhavi, and C. B. Thomas, "Multi-view breast thermogram analysis by fusing texture features," *Quant. Infr. Therm. J.*, Vol. 16, no. 1, pp. 111–28, Apr. 2019.
24. M. Abdel-Nasser, A. Moreno, and D. Puig, "Breast cancer detection in thermal infrared images using representation learning and texture analysis methods," *Electronics.*, Vol. 8, no. 1, pp. 100–18, Jan. 2019.
25. R. Ramya Devi, and G. S. Anandhamala, "Analysis of breast thermograms using asymmetry in infra-mammary curves," *J. Med. Syst.*, Vol. 43, no. 6, pp. 146–54, Apr. 2019.
26. S. Josephine Jeyanathan, A. Shenbagavalli, B. Venkatraman, M. Menaka, J. Anitha, and V. H. de Albuquerque, "Analysis of transform-based features on lateral view breast thermograms," *Circ. Syst. Signal Pr.*, Vol. 38, no. 12, pp. 5734–54, Jun. 2019.

AUTHORS



A. Arul Edwin Raj is currently working as an Associate Professor in Bethlahem Institute of Engineering, Karungal, Tamilnadu, India. He received his B.E and M.E degrees in electronics and communication engineering and Communication systems, respectively from Anna University, Chennai. He is currently pursuing his Ph.D degree from Anna University, Chennai. His current research interests include Medical image processing, Embedded and real time systems, Networking and pattern recognition.

Corresponding author. Email: arulme81@gmail.com



M. Sundaram is currently working as a Professor in Erode Sengunthar Engineering College, Perundurai, Tamilnadu, India. He completed his Ph.D degree from Anna University, Chennai, and he is a recognized supervisor for research under Anna University. He has published his research works in many national and

international conferences and journals. His research areas include thermal image processing for detection of breast abnormalities, quality analysis of edible items using Microwave energy. Nail image and Tongue image analysis for medical diagnosis, Pattern recognition and Machine Learning.

Email: cm.sundaram2011@gmail.com



T. Jaya is currently working as a professor and head of electronics and communication engineering department, CSI Institute of technology Thovalai, Tamilnadu, India. She completed her Ph.D degree from Sathyabama University, Chennai also she is a recognized supervisor for research under both Anna University and Sathyabama University. She has published her research works in many national and international conferences and journals. Her current research interests include Image Processing, Networking, Opto device, VLSI.

Email: jayacsiramesh@gmail.com